https://doi.org/10.1016/j.apenergy.2023.120878

Optimal yaw strategy and fatigue analysis of wind turbines under the combined effects of wake and yaw control

Ruiyang He*, Hongxing Yang*, Lin Lu
Renewable Energy Research Group (RERG), Department of Building Environment and Energy Engineering, The Hong Kong Polytechnic University, Hong Kong, China
*Corresponding author
E-mail address: hong-xing.yang@polyu.edu.hk (H Yang); ruiyang.he@connect.polyu.hk (R He)

Abstract

Yaw control is one of the most important farm-level active control strategies with the aim of power maximization and load mitigation. However, improper yaw strategies may induce a significant load increase on wind turbines (WTs) although a power enhancement can be achieved. Therefore, it is essential to conduct a comprehensive fatigue analysis of wind turbines under yaw control before proposing an optimal yaw control strategy. In this study, fatigue analysis of WTs under shear flow is conducted first under various environmental and yaw conditions. Bending moments at not only blade root and yaw bearing, but also non-rotating component like tower base are investigated. Furthermore, various wake conditions including both full wake and partial wake are generated to explore the combined effects of wake flow and yaw control. Different load trends and variation rates are obtained in the analysis. To determine the optimal yaw angle at different practical inflow and yaw conditions, a cost function is proposed by using resultant bending moments and further integrating loads at different components together. The results show that efficient yaw ranges all appear in the positive yaw direction and optimal yaw angle increases with the increase of inflow speeds. The comprehensive fatigue analysis and the proposed cost function for optimal yaw control in this work are expected to contribute to the research and applications of multi-objective active yaw control strategies and therefore to increase total power output while extending operation lifetime of wind turbines.

Keywords: *Wind turbine; Fatigue loads; Wake effects; Yaw control; Renewable energy*

Nomenclature

List of abbreviations

ABL	Atmospheric boundary layer
AWC	Active wake control
AYC	Active yaw control
BR	Blade root
D	Rotor diameter
DEL	Damage equivalent load
IFFT	Inverse Fast Fourier Transform
LES	Large eddy simulation
TB	Tower base
TI	Turbulent intensity
WT	Wind turbine

List of symbols

α	Angle in load rose
γ	Yaw angle
γ_{opt}	Optimal yaw angle
DEL_{BR}	DEL at blade root
DEL_{Yawing}	DEL at yaw bearing
DEL_{TB}	DEL at tower base
D_{total}	Total damage
i	Blade number
i_s	i-th sector in load rose
L_i^R	load range of i-th cycle about a load mean
L_i^{RF}	Cycle's load range about a fixed value
L^{ult}	Ultimate design load
L^{MF}	Fixed load mean
m	Wöhler exponent
N_i	Number of cycles to failure
N_s	Total number of sectors
n_i	Cycle count

1. Introduction

The utilization of wind energy is experiencing a globally real boom under the background of decarbonization. According to the latest Global wind report [1], a new installation of almost 94 GW of wind power is achieved in the past 2021, achieving a rapid growth rate of 12%. Meanwhile, the cluster development of wind power leaves most wind turbines (WTs) in the wake flow, which is detrimental to the power extraction and structural stability of WT components [2].

Active wake control (AWC) is a kind of strategy to intentionally mitigate the wake effects on downstream WTs, in which active yaw control (AYC) is the most promising one [3]. By horizontally deflecting the wake away from downstream WTs, AYC is expected to maximize the power generation of the whole wind farm while optimizing the fatigue loads of WTs [4]. However, improper yaw control on WTs may induce a significant increase in fatigue loads. Therefore, it is essential to fully characterize the fatigue loads of critical turbine components under yaw control.

Damiani et al. [5] characterized the fatigue load of wind turbine components under yaw conditions and gave multiple factors that contributed to the load trends. A two-turbine case concerning yaw control is carried out by yawing the first WT [6]. The study proved its capability of power enhancement while finding the potential of load mitigation in some fatigue representatives. Kragh and Hansen [7] investigated the wind shear effect on blade load and concluded that when the shear exponent is larger than 0.2, it would have no effect on optimal yaw angle. As for the effect of turbulent inflows, blade load alleviation due to yaw control was found more pronounced at low turbulence levels, while the load of non-rotating components may be penalized. Whereas, study from Ref. [8] declared that in positive yaw direction, the fatigue load of both the rotating components including blade, drivetrain, and yaw bearing as well as the non-rotating tower can be mitigated with yaw offset. By using the self-developed free vortex method, Shen et al. [9] also proved the load reduction of root flapwise moment with yaw offsets from 0° to 60°. On the contrary, Jeong et al. [10] denied the benefit of yaw control in terms of fatigue load. Their research indicated that yaw effects can induce significant load variation and therefore are detrimental for the structural stability. Similarly, a research from Ke et al. [11] suggested that yaw operation can considerably shorten the fatigue life of WT components, especially the blade root. As conflicting conclusions still remain, the structural performance of WTs under yaw control needs to be further investigated. More importantly, it is insufficient to study the fatigue load characteristics of yawed WT under shear inflow conditions alone.

In most cases, operating WTs are located in the wake flow of upstream WT and yawing these WTs can even benefit more for the total power output due to the secondary steering effect [12]. Consequently, fatigue analysis of yawed WTs under the wake effect is especially necessary. By using large eddy simulation (LES) coupled with OpenFAST, Chanprasert [13] investigated the fatigue loads of four in-line WTs under yaw dynamics. Sun et al. [14] quantified the fatigue caused by wake steering and full wake flow through OpenFAST and 3D analytical wake model. Then a polynomial function is proposed as a rapid fatigue prediction tool for the further multi-objective yaw optimization within wind farms. Urbán et al. [15] comparatively analyzed the blade flapwise load at three downstream locations. The results showed that for full wake conditions, low ambient turbulence is beneficial for load alleviation under yaw control. By analyzing the power output and yaw damage equivalent load (DEL) of three aligned WTs under yaw control, Lin and Porté-Agel [16] concluded that yawing the first WT with a small angle is not cost-effective since only a slight power enhancement can be achieved at a cost of significant yaw DEL increase. Additionally, a wind farm with constant 4D (D denotes rotor diameter) streamwise distance and several lateral positions was used to carry out wind tunnel tests and make a comparison based on yaw moment [17]. However, most studies only investigated the load trends of downstream WT under the deflected wake of upstream yawed WT but not the yawed downstream WT itself. Moreover, WT layouts that are responsible for wake effects generation and the studied fatigue representatives under these circumstances are limited in the current research. Therefore, there is a lack of comprehensive study on the combined effects of wake and yaw control on fatigue loads of WTs.

In order to efficiently employ the active yaw control throughout the whole wind farm, the optimal yaw angle of each WT should be determined based on power output and fatigue loads. Bossanyi [18] proposed a cost function by giving the bending moments at tower base and blade root 10% weighting and comparing it to the power enhancement. van Dijk et al. [19] defined the problem by directly adding the flapwise and edgewise load together and then adding the power with an unknown factor. After that, the optimal yaw settings can be

determined by solving the unknown factor with a quasi-Newton optimization algorithm. By using Pareto optimal strategy, Lin and Porté-Agel [16] calculated the optimal yaw offset with the goal of power maximization and yaw moment minimization. Urbán et al. [15] considered only the yaw strategy without power losses and therefore simplified the optimal yaw angle as the angle that has minimal flapwise DEL while keeping the power constant. Similarly, Ennis et al. [20] adopted the flapwise DEL as fatigue representative and defined the optimal yaw angle as the angle that has a minimal ratio of normalized flapwise DEL to power yield. In addition to the optimization goal of load minimization, some researchers valued the minimal variation of load in yaw control. Akay et al. [7] obtained optimal yaw angle by minimizing the azimuthal variation of flapwise moment and further simplifying the problem by finding the minimization of the variation of inflow angle. However, multiple fatigue loads are not reasonably integrated and directly adding the fatigue loads at two directions is overly conservative. Besides, in most cost functions, only one kind of fatigue load is considered, mainly the blade root load in the flapwise direction, which is inadequate.

To fill the research gap clarified above, the main contributions of this study are listed as follows. (1) A turbulent, time-series 3D atmospheric boundary layer (ABL) generator is built up and its combination with dynamic wake meandering (DWM) is responsible for wake modelling, which ensures an accurate description of the realistic flow field. (2) Under the inflow conditions including various wind speeds, turbulent intensities, and shear effects, a comprehensive fatigue analysis of yawed WT is conducted concerning the critical turbine components from the blade root to non-rotating parts. (3) The combined effects of wake and yaw control on these fatigue loads are analyzed with typical full wake and partial wake layouts to reveal their relevance. (4) An optimal yaw control strategy is proposed by considering the resultant bending moments at critical components. Then, an efficient yaw control range is defined based on the proposed cost function.

2. Methodology

2.1 NREL 5MW wind turbine model

The NREL 5MW baseline WT (NREL 5MW hereafter) is selected as the target wind turbine model, which is a conventional three-bladed upwind wind turbine with a utility scale. The hub height is 90m and the blade diameter is 126m. The cut-in, rated and cut-out speed is 3m/s, 11.4m/s and 25m/s, respectively. For a more detailed description of the NREL 5MW, please refer to [21]. As for the yaw direction, positive yaw angles are defined as clockwise direction when looking down from the upstream to downstream while the negative yaw angles are considered counter clockwise. A sketch of yaw direction is illustrated in Fig. 1. As mentioned in Ref. [22], with yaw angles above 30°, the power loss of yawed WT cannot be compensated by the power enhancement from the downstream WTs. Therefore, in this study, yaw angles from -30° to 30° with an interval of 10° are suitable to be investigated.

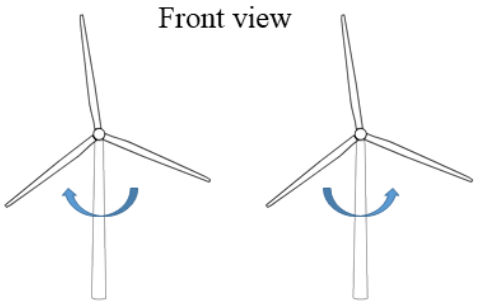

Fig. 1 A demonstration of positive yaw offset (left) and negative yaw offset (right).

2.2 Wind field modeling

To ensure the generality of the fatigue analysis on wind turbines under active yaw control, the wind field should be modelled properly. A variety of turbulent free-stream wind fields are generated by specifying meteorological boundary conditions with typical values [23]. Meanwhile, different kinds of wake conditions, including both full wakes and partial wakes, are modelled by specifying typical interval spacings [14,15].

2.2.1 Generation of free-stream wind field

The full-field turbulent three-dimensional wind is generated by Turbsim [24]. In Turbsim, by making use of inverse Fast Fourier Transform (IFFT), classical wind spectra, like Kaimal spectrum and Von Karman spectrum, can be transferred to stochastic, turbulent, full-field wind data with time-series three components of speed vectors. Examples of the generated time-varying turbulent wind speed at hub height and rotor plane are displayed in Fig. 2. According to the IEC standard [25], a 10-min continuous structural signal is required to generate short-term damage equivalent load. Therefore, in this study, the time duration of turbulent wind field generated by Turbsim is set as 800s with IEC Kaimal spectral model. Only the aeroelastic performance corresponding to the latter 600s is adopted to avoid the initialisation effects of the tested wind turbine.

Once the wind spectrum model and time duration have been set, the ABL can be determined by specifying the wind speed at hub height, turbulent intensity, and the shear exponent. Wind speeds that are likely to benefit total power generation through active yaw control are adopted in this study to investigate the fatigue loads, specifically from 9m/s to 17m/s in 2m/s intervals. Then, 5% and 14% represent low and high turbulent intensities, respectively, to reveal the effect of turbulence ABL on the WT operating yaw control. Lastly, shear exponents from 0.1 to 0.26 are employed to cover a wide range of surface roughness. For more details about the ABL setup, please refer to Table. 1.

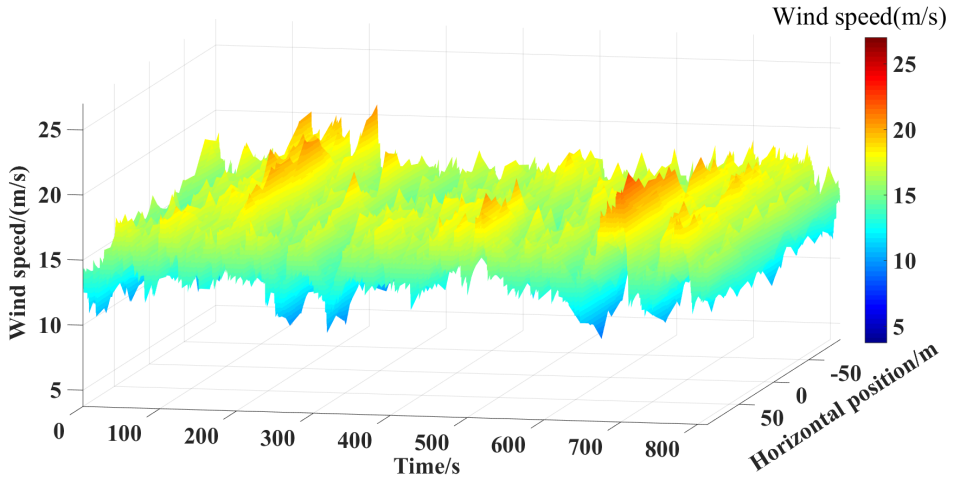

(a) Velocity variation at hub height.

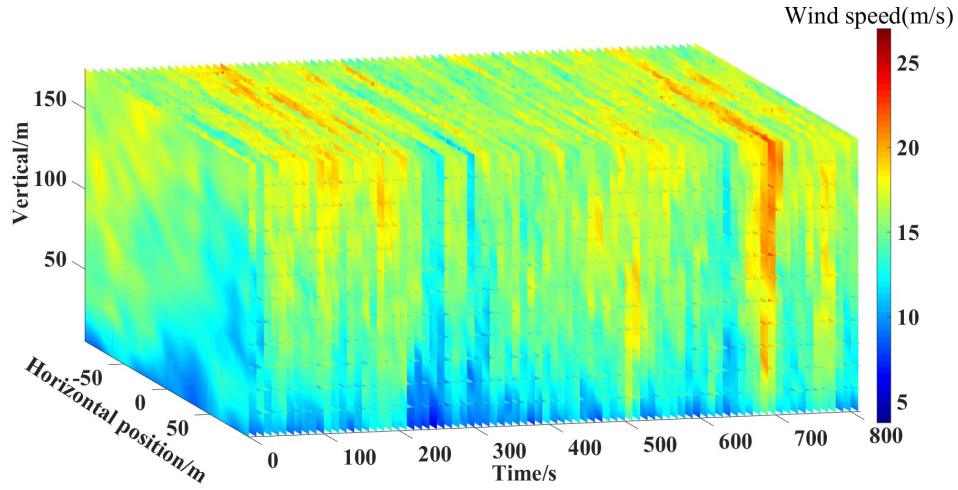

(b) Velocity variation at rotor plane.

Fig. 2 An example of time-series turbulent wind speed used for simulation.

2.2.2 Generation of wind field with various wakes

Except for the isolated yawed wind turbine, the fatigue analysis needs to be extended to the main situations since most wind turbines in a wind farm are exposed to wake flows. In order to accurately estimating the increased fatigue loads due to wake effects and elucidate the correlation between wake effects and yaw control on the structural performance of downstream wind turbines, a reliable and accurate tool for wake prediction is highly essential.

In this study, the advanced dynamic wake meandering model (DWM) [26] coupled in FAST.farm [27] is employed to generate wake flow, which models the wake evolution as a passive tracer and has been successfully verified with large eddy simulation (LES) and full-scale measurements [28,29]. As shown in Fig. 3, the DWM model consists of three sub-models: namely, the model for computing quasi-steady wake deficit evolution via the thin shear-layer approximation of the Reynolds-averaged Navier-Stokes (RANS) equations, a model for predicting wake meandering process induced by large turbulent eddies, and a model for determining the added wake turbulence generated from the turbulent mixing in the wake.

By using the same DMW wake model, Urban and Larsen et al. [15] carried out a two-turbine experiment: the first WT is responsible for generating various full wake and partial wake conditions. Similarly, Fleming et al. [6] simulated fully waked situations by tandemly spacing one WT 7D apart from its downstream counterpart. Then, Gebraad et.al [30] extended the above setup to generate partial wakes by using one upstream WT.

The advantage of using one upstream WT to generate wake effects is that the wake conditions can be clearly characterized and therefore the resulting load variation of downstream WT can be summarized in a qualitative way. Moreover, the multiple combinations of streamwise and spanwise spacings between two WTs are able to meet the complex requirements of generating various wake situations. On the other hand, based on the conclusion mentioned in Ref. [31], the wake deficit remains below 0.58 even for highly densely populated wind farms, which means that the wake deficit in superimposed wake can be reasonably modelled by a single WT upstream.

Consequently, one upstream wind turbine is responsible for generating various wakes depending on the relative spacing between WTs, which can be decomposed into streamwise spacing and spanwise spacing. WTs with only streamwise spacings denote that the downstream WT is exposed to full wake conditions while a combination of streamwise and spanwise spacings can produce various partial wakes. In this study, typical streamwise

spacings from 4D to 7D (D denotes the length of WT diameter) and the effective spanwise spacings from -1D to +1D with an increment of 0.25D are adopted to provide realistic wake conditions in wind farms. For more details about simulation settings, please refer to Table. 1.

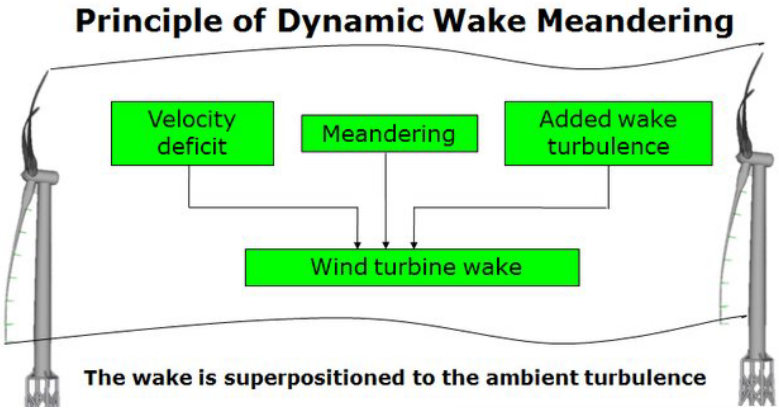

Fig. 3 Overview of the three sub-models of the DWM model. Source:[32] with permission.

Table 1. Environmental and operational conditions employed in simulations.

Parameter	Value	Number
Velocity	9 m/s, 11 m/s, 13 m/s, 15 m/s, 17 m/s	5
Turbulent intensity	5%, 14%	2
Shear exponent	0.1, 0.14, 0.18, 0.22, 0.26	5
Yaw angle	0°, ±10°, ±20°, ±30°	7
Streamwise distance	4D, 5D, 6D, 7D	4
Spanwise distance	0D, ±0.5D, ±0.75D, ±1D	7

2.3 Fatigue load computation

The structural responses of the target WT under yaw control is calculated by an aero-servo-elastic code called OpenFAST (for single WT) [33,34] or FAST.farm (for multiple

WTs) [27], which can provide full nonlinear and high-fidelity simulation. Free wind vectors generated by Turbsim or realistic wakes generated by DWM model are fed to aeroelastic code to compute time-series fatigue structural signals. Considering that fatigue fractures usually happen in the root places that are subjected to high alternating shear stress, two components of bending moment at blade root and tower base are selected as fatigue representatives.

It should be noted that using the larger component to represent the maximal load at the target position is unconservative, while directly adding the two components is overly conservative. To reasonably represent the bending moment at these places, a resultant bending moment should be calculated via load rose [5]. As denoted below:

$$\alpha = (i_s - 0.5) * 180 / N_s \tag{1}$$

$$Load(i_s) = Load0 * COS(\alpha) + Load90 * SIN(\alpha) \tag{2}$$

where α is the calculated angle in the load rose; i_s is the i-th sector; N_s is the total number of sectors. Then the resultant load at each sector can be computed by the Eq.(2). The maximal one among sectors is selected as the representative bending moment. According to the IEC standard, 15° resolution with 12 sectors is adopted for the load rose in this study [35].Besides, yaw moment at yaw bearing are also selected in this yaw-related fatigue analysis.

In order to conduct fatigue analysis and characterization, as shown in Fig. 4, the time-series fluctuating load signals are converted to damage equivalent load (DEL) by rain flow counting algorithm [36] with the assumption of linear accumulation of each load cycles (known as Miner's rule [37]). As expressed by Eq. (3):

$$D_{total} = \sum_i \frac{n_i}{N_i\left(L_i^{RF}\right)} \tag{3}$$

where D_{total} denotes the total damage; n_i is the cycle count; N_i is the number of cycles to

failure due to the cycle load range L_i^{RF} over a fixed load-mean value. According to the S-N curve [38], the cycles to failure N_i and load range L_i^{RF} have th relationship as follows.

$$N_i = \left(\frac{L^{ult} - \left| L^{MF} \right|}{\left(\frac{1}{2} L_i^{RF} \right)} \right)^m \tag{4}$$

where L^{ult} is the ultimate design load of the component under consideration; L^{MF} is the fixed load mean; m is the Wöhler exponent, which depends on the material of the specific turbine components. In this study, the Wöhler exponent for blade (made of composite) is 10 and that for tower and yaw bearing (made of steel) is 4.

The actual load cycles occur over a spectrum of the load means instead of the fixed mean load assumed in the above equations. Consequently, the Goodman correction model [38] is needed to adjust the load ranges of fatigue cycles L_i^{RF} to treat the data as if each cycle occurred about a fixed mean load.

$$L_i^{RF} = L_i^R \left(\frac{L^{ult} - \left| L^{MF} \right|}{L^{ult} - \left| L_i^M \right|} \right) \tag{5}$$

where L_i^R is the load range of i-th cycle about a load mean of L_i^M.

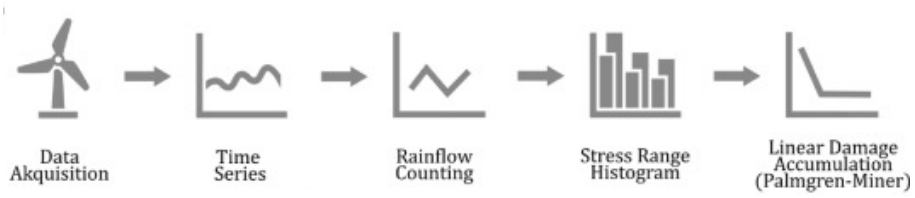

Fig. 4 Standard fatigue calculation process. Source: [35] with permission.

3. Fatigue analysis of yawed wind turbine under free streams

The effects of inflow conditions on fatigue loads under active yaw control are comparatively analyzed. The fatigue loads of critical turbine components that are suffered

from alternating shear stress are selected, including flapwise and edgewise moments at blade root, yaw moment at yaw bearing, and side-to-side and fore-after moments at tower base. For the ease of comparison, all the results are normalized by the corresponding structural load under aligned and the most moderate inflow condition.

Fig. 5 displays the variations of edgewise DEL at different inflow and yaw conditions. As expected, the variation range of edgewise moment is moderate, ranging from 0.9 to 1.1 at low TI and 1.15 at high TI. Surprisingly, it is observed that the high wind speeds, such as 15m/s and 17m/s, induce relatively little edgewise load compared to small wind speeds and can largely mitigate the load variation caused by yaw operations. Edgewise DEL at 11m/s and 13m/s decrease monotonically with yaw offset and has a comparatively large amount of variation. On the contrary, the load variation has the opposite trend at high speeds like 17m/s, which may be caused by the increase in pitch angle. As can be seen from the comparison between the two sub-figures, turbulence level is found to have little effect on both load trend and load magnitude of edgewise DEL.

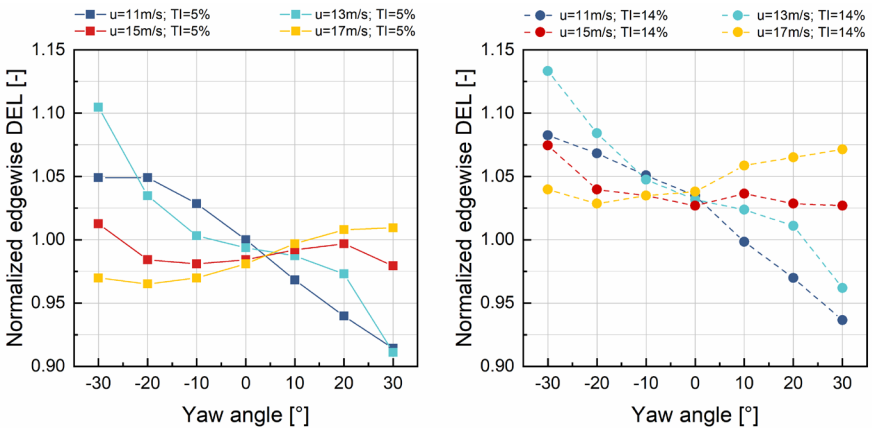

Fig. 5 Normalized flapwise DEL as a function of yaw angle for different inflow speeds and turbulence.

Fig. 6 illustrates the trend of flapwise DEL with yaw angle, wind speed, and turbulent intensity. From the negative yaw angles to positive ones, the load trend of flapwise DEL displays an asymmetric decrease first and then increase. However, the inflection point at

which asymmetry occurs is variable. For relatively high wind speeds like 15m/s and 17m/s in this study, the inflection points tend to occur far from 0° while the speeds below this value have inflection points near the 0°, which means that increasing inflow speeds can exacerbate the asymmetry of the load variation. The asymmetric trend of flapwise DEL with yaw offsets can be explained by the wind shear effect counteracting the advancing and retreating blade effects [39]. Besides, when it comes to the effect of turbulence on flapwise DEL, it can be observed that the increased turbulence level can significantly increase the load magnitude, in which high-speed cases increase greater. The increase in load at high speeds is in the order of 2-3 times while at relatively low speeds the increase is in the order of 1-2 times.

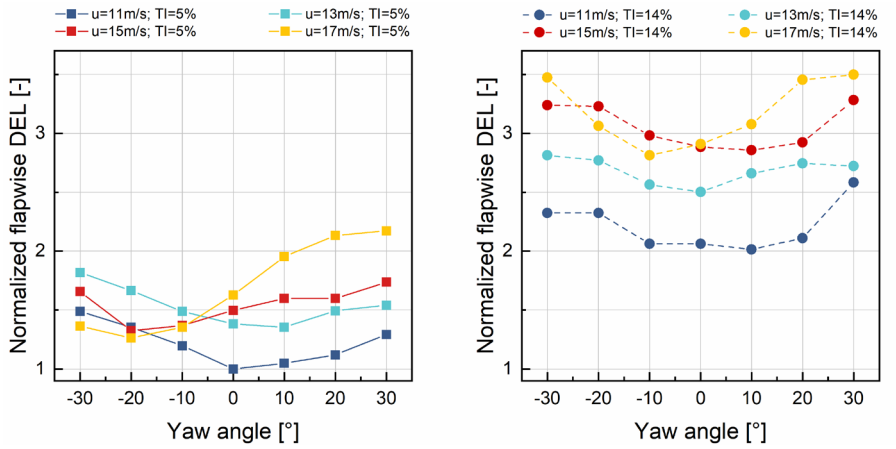

Fig. 6 Normalized edgewise DEL as a function of yaw angle for different inflow speeds and turbulence.

The variation of yaw bearing DEL under active yaw control is shown in Fig. 7. As expected, the load trend at low TI shows an approximately symmetrical concave curve distribution with its lowest point appeared at the non-yawed condition. With the increase of yaw angle, yaw bearing will be subjected to more structural load due to the increasingly imbalanced forces and the rotation of rotor. On the contrary, the load trend at high TI is relatively flat, which can be explained by the fact that the dominance of high TI on yaw moment diminishes the effect of yaw operation. Also, the increased turbulence intensity magnifies the difference in yaw DEL at different speeds compared to those under low

turbulence. In general, the fatigue increment is more significant at high velocities by a factor of 2.5 times.

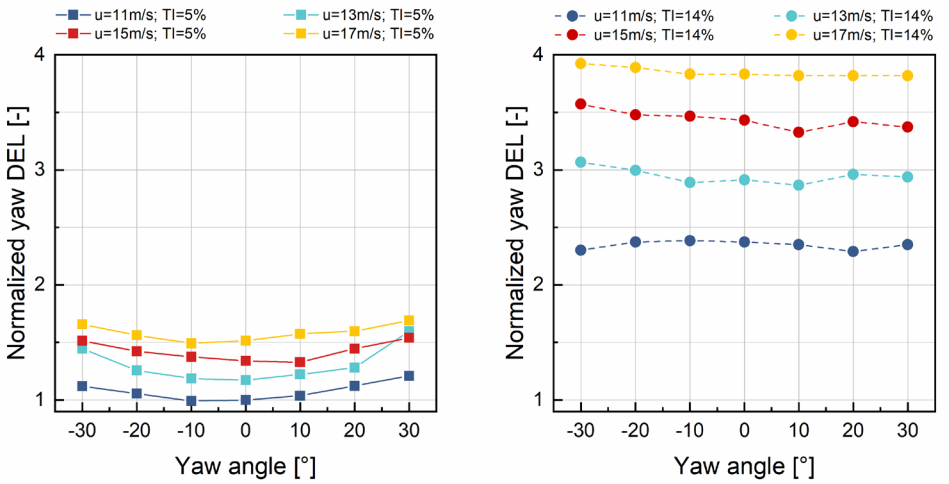

Fig. 7 Normalized yaw DEL as a function of yaw angle for different inflow speeds and turbulence.

The fatigue loads at non-rotating components like tower base are also analyzed under active yaw control. The variation of side-to-side loads as a function of inflow condition and yaw angle is illustrated in Fig. 8. The side-to-side motion is usually thought to be caused by mechanical and electrical disturbance, but in fact, yaw misalignment would also cause lateral bending moment to increase. With the increase of yaw offsets, the turbine tower is exposed to greater bending moment in the lateral direction, and this phenomenon is exacerbated by high speed and large turbulence. As seen in the figure, the maximal side-to-side load appearing at 17m/s with 14% turbulent intensity is almost 5 times larger than the 7m/s with 5% turbulent intensity. Also, the large turbulence induces the variation of load trend compared with the roughly symmetrical one under low turbulence level. These changes indicate that the side-to-side moment is susceptible to inflow conditions.

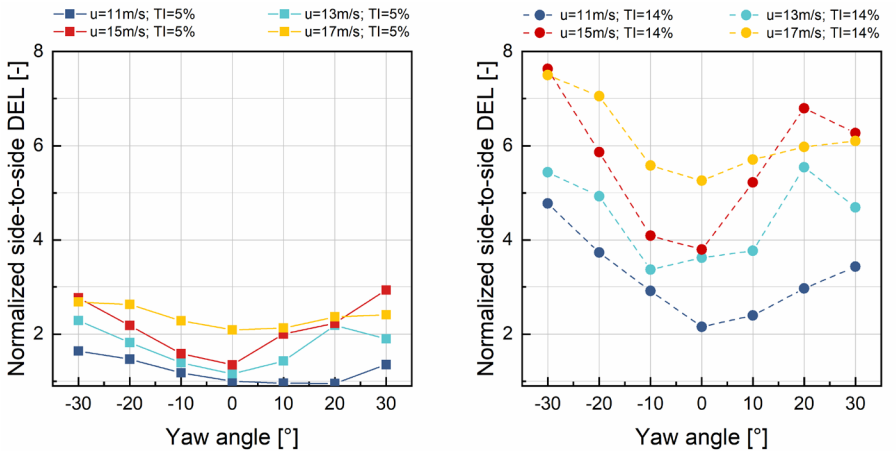

Fig. 8 Normalized side-to-side DEL as a function of yaw angle for different inflow speeds and turbulence.

Fig. 9 shows the variation of fore-after DEL at tower base. Compared with side-to-side load, the moment in fore-after direction is relatively flat with yaw angle, especially at the low TI condition, which means it is less sensitive to the yaw misalignment. Since fore-after DEL is mainly caused by inflow wind speed, yawing the rotor and nacelle would not largely benefit the load alleviation of tower base in fore-after direction. In general, the load magnitude of fore-aft DEL at low TI is similar while the case of 11m/s and other cases shows disparity at high TI condition. The overall increment caused by turbulent intensity is not as large as the side-to-side DEL.

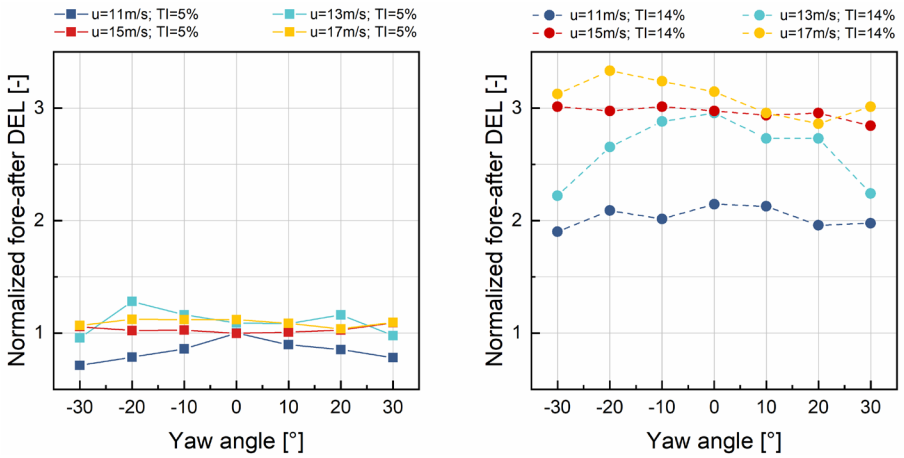

Fig. 9 Normalized fore-aft DEL as a function of yaw angle for different inflow speeds and

turbulence.

The normalized power output considering inflow conditions and yaw operations is shown in Fig. 10. The power trend with yaw angle is strictly symmetrical about the 0°, which indicates that the yaw direction has no bearing on the changes in power generation. When the incoming wind speed is less than the rated one, any adjustment to the angle of rotor plane will result in a loss of power. As the yaw angle increases, the thrust force harvested by wind turbine becomes less and therefore the lower the power output. With the increase of wind speed above the rated value, the yaw control range without power loss will be gradually enlarged until the full range of yaw operation. When the inflow speed is slightly larger than the rated value, for example 13m/s, the loss of thrust force due to small angle of yaw operation still allows the WT to maintain its power at rated value. However, as the yaw angle continues to increase, the loss of rotor thrust is no longer sufficient to be compensated for by the inflow velocity that only a little more than the rated value, not mention that pitch control also reduces the capacity of blades to harvest energy. For the cases where the inflow velocity is much greater than 11.4m/s, such as 15m/s and 17m/s in this study, yaw misalignment can be applied without power losses. When it comes to the influence of turbulence, although the increment in turbulence level can strongly influence the fatigue loads, it seems that it has little effect on the power output.

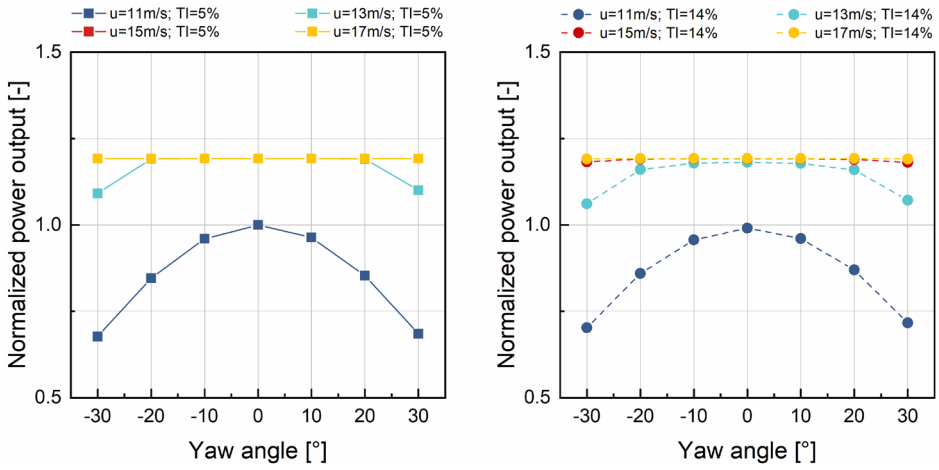

Fig. 10 Normalized power generation as a function of yaw angle for different inflow speeds

and turbulence.

Fig. 11 shows the effects of shear inflow on fatigue loads and power output. Shear exponents from 0.1 to 0.26 were employed while keeping the wind speed and turbulent intensity constant. The results demonstrate that shear effects have a remarkable influence on flapwise moment. This is because once the shear effect becomes more pronounced, the rotating blade will experience greater alternating stress on each cycle due to the high shear inflow wind speed from top to bottom. Also, the shear effects magnify the load difference between yaw misalignments. When the shear exponent equals to 0.26, the flapwise DEL at -30° is more than 50% larger than that at 30°, whereas the difference is only about 13% when the shear exponent is 0.1. The moment at yaw bearing is also significantly influenced by shear effects. The maximal value for all yaw angles appears at the shear exponent of 0.26, with the largest discrepancy from -30° to 30° reaching 28%. On the other hand, the fatigues at tower base are less affected by the variation of shear exponent, which can be explained by the relatively moderate variation of wind speeds experienced by tower base due to the changes of shear exponents. Besides, based on the analysis of Fig. 8 and Fig. 9 (f), the power yield is less affected by shear exponent and turbulent intensity. Only the wind speed at hub height and yaw angle are sufficient to estimate the electrical power generation. It should be noted that although the shear exponent has no effect on power output, it does affect the fatigue loads of wind turbines and will eventually indirectly affect the total power generation of a WT during its lifespan.

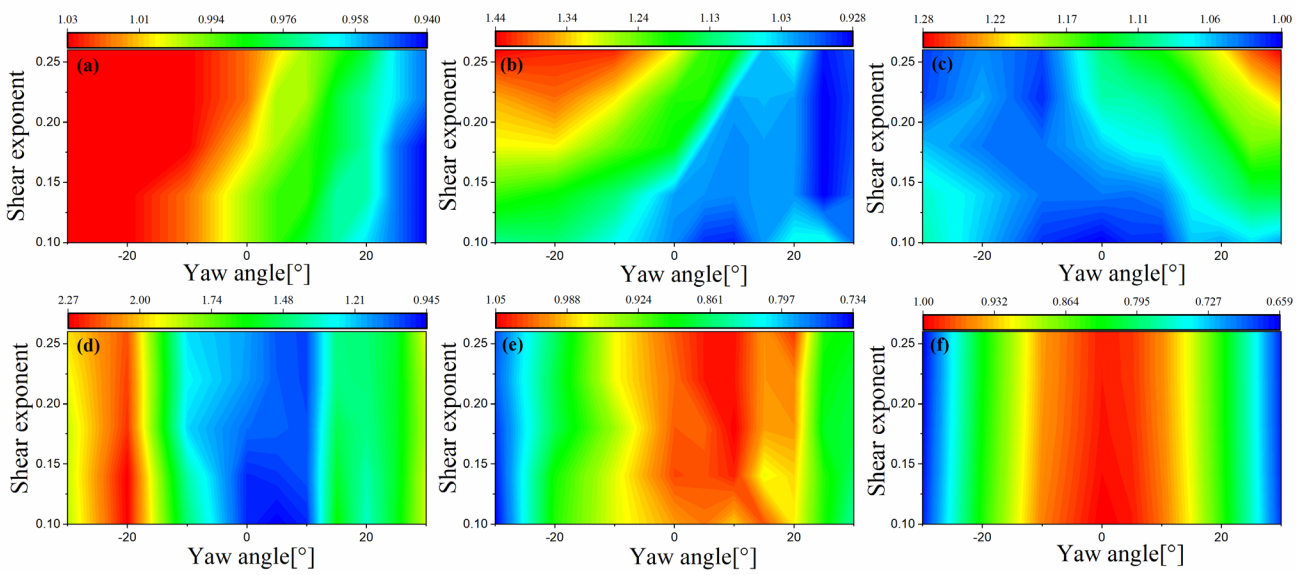

Fig. 11 Normalized fatigue and power as a function of yaw angle for different shear effects. (a) Normalized edgewise DEL. (b) Normalized flapwise DEL. (c) Normalized yaw DEL. (d) Normalized side-to-side DEL. (e) Normalized fore-after DEL. (f) Normalized power output.

4. Fatigue analysis of the combined effect of wake and yaw control on WT

Since most wind turbines in a wind farm are sunk into the wake of their upstream counterparts, the downstream wind turbines under yaw control are exposed to complicated wake profiles from upwind while deflecting their wakes. Therefore, it is essential to investigate the combined effects of wake flow and yaw misalignment on fatigue loads and power output. As demonstrated in Section 2.2.2, various wake effects can be generated by different layouts, which can be broken down into streamwise and spanwise distance. The streamwise distance is responsible for full wake adjustment and the spanwise distance can control the overlapping area of partial wake. For completeness, all comparative studies in this section use the same free-flow condition, namely 9m/s at hub height with a power-law shear exponent of 0.1 and an ambient TI of 5%. Please noted that since the aim of this study is to conduct fatigue analysis of WTs under the combined effect of wake and yaw offsets, only the downstream WT is under yaw operation while the upstream WT is responsible for wake generation.

4.1 Yawed wind turbine under full wake

4.1.1 Full wake characterization

To model the yawed wind turbine under full wake, two WTs are tandemly arranged with respect to the inflow direction. The streamwise distances are adjusted in a typical spacing range while keeping the spanwise distance as zero. To elucidate the wake effects on yawed wind turbines, wake characteristics including turbulent level and normalized inflow speed at hub height need to be qualified first.

Table 2 displays the wake turbulent intensities and speeds experienced by downstream WT, in which the interval spacing in streamwise direction ranges from 4D to 7D. The ambient turbulent intensity is set as 5% and the inflow wind speed is set as 9m/s at hub height. As demonstrated in Section 2.2.2, the wake field is generated by realistic turbulent wake model and the therefore wake characteristics shown in Table 2 are averages of 600s. It is found that the added turbulence is approximately 60% of the original value and reaches its peak value at about 5D. The turbulence trend along streamwise direction is rather flat from 4D to 7D, which means the turbulence level of wake would not recover as fast as the speed. As shown in Table 2, the wake deficit at the hub center of downstream WT is 0.38 at 4D distance and then reduce to 0.28 at 7D, signifying a noticeable recovery of wake speed at hub center. In contrast, the approximately symmetrical wake flow at left and right edges recovers relatively gently, especially from 5D to 7D. Overall, with the increasing of streamwise spacing, the wake depth (defined by the speed difference between hub center and both sides) decreases gradually, which means that the downstream WT is exposed to a relatively less inhomogeneous flow field. Therefore, it can be concluded that increasing the streamwise distance can improve inflow condition in terms of wake speed but have little effect on turbulence level.

Table 2 Wake characteristics at different full wake positions.

Streamwise position	Free flow	4D	5D	6D	7D

Turbulence intensity [%]	5.0	8.0	8.2	8.2	8.1
Normalized wind speed at left edge [-]	0	0.81	0.85	0.86	0.87
Normalized wind speed at hub center [-]	0	0.62	0.65	0.69	0.72
Normalized wind speed at right edge [-]	0	0.81	0.84	0.86	0.87

4.1.2 Fatigue analysis of yawed wind turbine under full wake

Fatigue loads of a tandemly located downstream yawed wind turbine are shown in Fig. 12. Two downstream distances, 4D and 7D, are selected to make a comparison with WT under sheared flow. For the ease of comparison, all representatives are normalized by the corresponding fatigue on the upstream WT without yaw operation. Besides, to quantify the increase or decrease of fatigue loads due to the combined effects of wake and yaw control, variation rates at 4D and 7D are given based on the fatigue load on upstream WT at the same yaw offset.

According to the fatigue analysis in Section 3, the load trend of edgewise DEL is relatively moderate and the load magnitude remains almost constant. Moreover, the variation law of power output is also well grasped, that is, it is symmetrical about the zero yaw angle and only affected by the wind speed. So, it can be expected that as the spacing increases, the power output becomes larger but still lower than the power of upstream WT due to the wake deficit. Therefore, these two representatives are not included in the full wake comparative analysis.

As illustrated in Fig. 12(a), for all yaw offsets, flapwise moments of downstream WT at 4D are smaller than that of the upstream WT due to strong wake deficit, although the variation rate shows a gradual increase with yaw angle. The situation is different for the 7D distance. Flapwise DEL there shows greater values than upstream WT at positive yaw offsets, but smaller values at negative ones. It is worth noting that the load trends shown in WT under

wake are completely different from that of WT under sheared inflow. For 4D and 7D, the variation rates follow a similar trend with yaw angle, basically increasing monotonically, but with larger values at 7D. On the other hand, the trend of flapwise DEL of WT under free stream asymmetrically decreases first and then increases with yaw angle. Consequently, for yawed WTs under wake effects, negative yaw misalignments can significantly alleviate flapwise DEL compared with the positive yaw angles yet make the same contributions to wind farm power enhancement as positive ones.

The yaw DEL and its variation rate of WT under wake effects are shown in Fig. 12(b). It can be observed that in most cases, the yaw moment of WT under wake effects is larger than that under free flow, and yaw DEL at 7D tends to be larger. Considering the wake characteristics and yaw DEL analyzed in Section 3, the yaw moments at 4D become larger since the importance of added turbulence outweighs that of speed loss in wake flow. The yaw load increases further with spacing as the wake recovers in velocity with little change in turbulent intensity. Interestingly, the load trends of yaw DEL under the combined effects of wake and yaw control have totally opposite trends compared with those under solely yaw operation. At 4D and 7D, the maximum value of yaw load appears where no yaw misalignment is applied and decreases at a similar rate on both sides. However, the maximal yaw DEL of WT under free flow occurs at full yaw conditions, but the increment is smaller than that under wake effects.

The side-to-side DEL and the corresponding variation rates are demonstrated in Fig. 12(c). The fatigue load under wake effects is larger than that under free stream in most cases, although the relationship between load magnitude of 4D and 7D is unclear. The minimum values of side-to-side DEL all appear at unyawed conditions either under the combined effects or solely yaw operation, which means that wake characteristics may change the load trend, but the yaw offset has a dominant effect on the load variation. In general, the side-to-side load in the positive direction is lower than the load in corresponding negative yaw angles, indicating that a positive yaw misalignment could exert less influence on the lateral structural

responses at tower base when achieving the same wake steering effect. The variation rates of two spacings show a maximum value at -30° with 64% for 4D and 44% for 7D, respectively. Then the curves decrease first with the minimum value at -20° and increase with yaw angle.

Fig. 12(d) displays the fore-aft DEL under the wake effects and the corresponding variation rate. Compared to the fore-aft moment under free flow, the moments in wake flows are increased at all yaw offsets up to 64%, demonstrating that wake effects can considerably increase the fore-aft load at tower base. The increased load can be explained by the added turbulent intensity in wake and larger fore-aft vibration caused by non-uniform wake distribution. With the increase of yaw angle in the positive direction, the fore-aft loads at 7D are larger than those at 4D while, while the magnitude relationship would change after the yaw direction is reversed. In general, the load under wake flow tends to be relatively flat with yaw angle. The load under free flow is larger at small yaw offsets and smaller at larger yaw offsets though the variation is still small compared with the side-to-side moment. The variation rates at 4D and 7D also have a similar trend, decreasing first and then increasing with the minimum load increase at normal operating conditions. Therefore, large yaw offsets of a wind turbine in wake would aggravate the increase of fore-aft load.

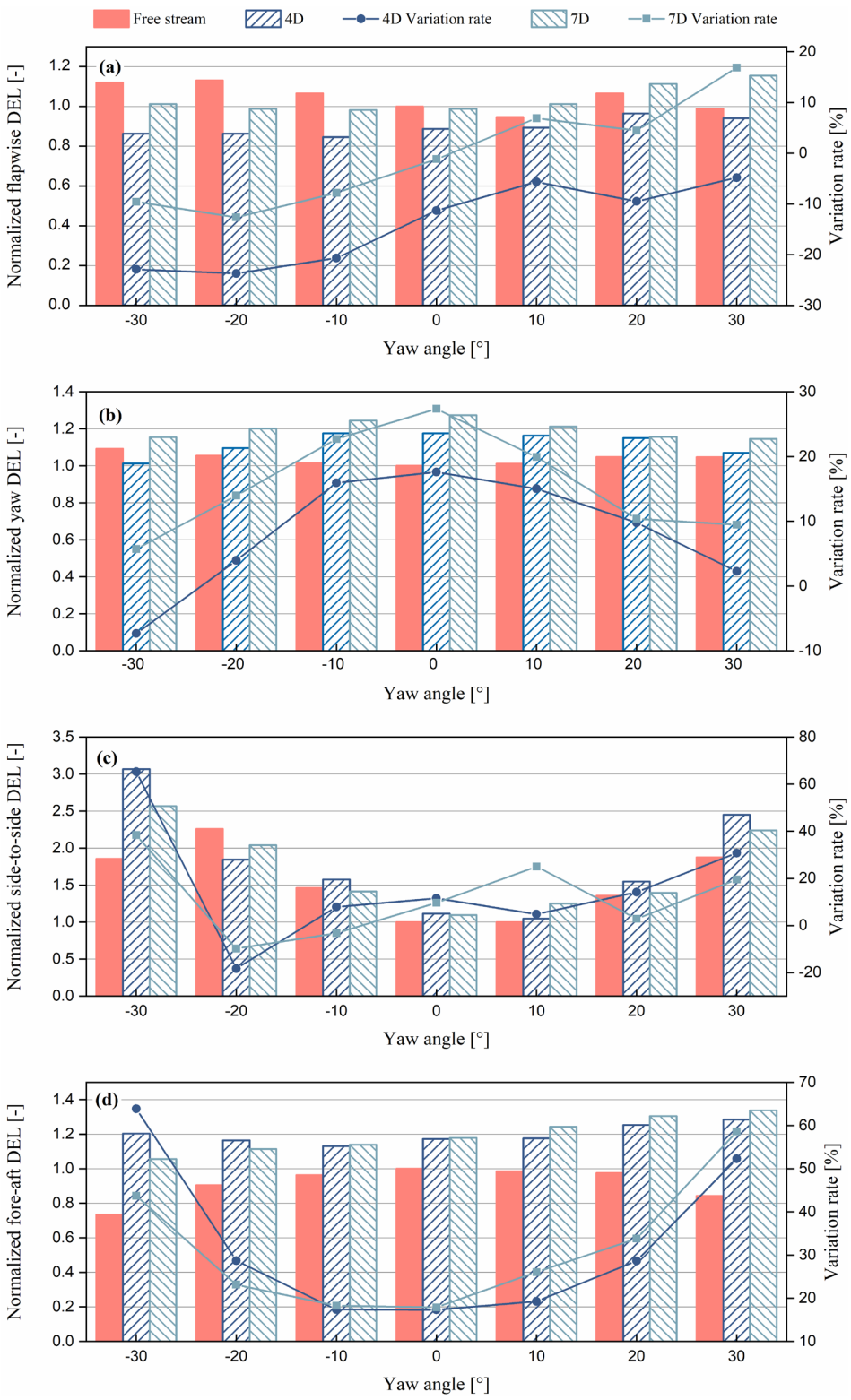

Fig. 12 Fatigue loads variation as a function of yaw angle under full wake effects.

4.2 Yawed wind turbine under partial wake

4.2.1 Partial wake characterization

Partial wake fatigue analysis adopts the same atmospheric state as full-wake cases while keeping the streamwise distance as 4D. The spanwise spacings are set as ±0.5D, ±0.75D, ±1D and are compared to full wake cases. The partial wake is characterized by using turbulent intensity and velocity at hub height via their 600s averages of the real time-series wake field. As displayed in Table 3, the turbulence levels at hub height decrease with spanwise position though a slight difference exists in two directions. On the other hand, with the increase of WT distance laterally, the wake profiles experienced by downstream WT are gradually changed from symmetrical Gaussian distribution to gradient distribution with a larger speed outside. The table below reflects that the gradient of the incoming flow on the left and right edges of rotor is at its maximum at ±0.5D and decreases with increasing spanwise spacing. At ±1D distance, the velocity of at least half of the swept area has been recovered to the free stream inflow condition. Compared with full wake conditions, the asymmetric wind distribution and lower turbulent intensity will inevitably result in different load characteristics for the rotor and tower.

Table 3 Wake characteristics at different partial wake positions.

Streamwise position	-1D	-0.75D	-0.5D	0D	0.5D	0.75D	1D
Turbulence intensity [%]	5.48	5.62	6.36	8.01	6.76	6.08	5.78
Normalized wind speed at left edge [-]	0.81	0.66	0.63	0.81	1	1	1
Normalized wind speed at hub center [-]	1	0.96	0.81	0.62	0.80	0.96	1
Normalized wind speed at right edge [-]	1	1	1	0.81	0.62	0.65	0.80

4.2.2 Fatigue analysis of yawed wind turbine under partial wake

Fig. 13 exhibits four fatigue load channels versus yaw offsets under various partial wake conditions. Please note that since the aim of misaligned operation is to deflect the wake towards free stream, only the positive yaw operations of downstream WT with positive lateral displacement are considered and vice versa. For the same reasons as explained in full-wake cases, the variation of edgewise DEL and power output with yaw offset are not presented as well.

In Fig. 13(a), it is found that flapwise DEL under partial wake conditions are mostly greater than full wake in each misaligned layout, in which the largest increment up to 75% appears at non-yawed condition. The increased flapwise moment is caused by exacerbated vibration of blades in each cycle due to the imbalance of inflow wind. Although here exhibits a decrease in turbulence intensity with lateral displacement, the results show that asymmetric inflow distribution outweighs the reduced turbulence in blade fatigue. Furthermore, partial wake induces changes in load trend with yaw offset. For WTs under sheared flow, the flapwise DEL decreases first and then increases with yaw offset and its minimum value appears at a certain yaw angle close to 0° due to wind shear. For WTs under partial wake, however, the maximum flapwise load at all lateral positions arise at 0° and then decreases. The comparison results indicate that yawing rotors towards the outside could provide more uniform wind distribution and therefore benefit the decrease of fatigue at blade root.

As yaw DEL shown in Fig. 13(b), lateral displacement of WT under wake increases the fatigue moment at yaw bearing to varying degrees. Like the load trend of full wake, cases of partial wake also have a maximum at the aligned condition and then decrease at both sides, which is opposite to the situations with sheared inflow. With the increase of spanwise distance on both sides, the yaw moment increases first and then decreases with the most significant increase taking place at $\pm$0.75D. That is because, at $\pm$0.75D distance, rotors experience approximately half wake and half sheared flow, any rotor deflection could help alleviate the

fatigue of yaw bearing under this circumstance.

When it comes to the variation of side-to-side DEL in partial wake conditions, as illustrated in Fig. 13(c), ±1D cases that experience less wake flow are mostly smaller than both other partial wake and full wake cases. With the increase of spanwise spacing, the maximum appears at -0.5D for negative yaw operation and appears at 1D for positive yaw operation. All partial wake cases follow the similar load trend to the full wake case, decreasing first with minimum value appearing at non-yawed or slightly positive yaw condition and then increasing. In either full wake or partial wake conditions, negative misalignments produce larger fatigue side-to-side load than the positive counterparts, while the discrepancy tends to be mitigated with increasing spanwise distance.

Compared with the variation of side-to-side DEL, fore-after moments shown in Fig. 13(d) have a relatively small magnitude of variation since they are less sensitive to mechanical vibration. Partial wake conditions that are largely affected by wake flow like ± 0.75D and ±0.5D have greater fore-after load than the full wake case, although the discrepancy in positive misalignment is more noticeable. Unlike the situation of side-to-side moment, positive yaw operations lead to a remarkable load increase for all lateral displacements. Interestingly, compared with the full wake counterpart, partial wake layouts also change the load trend with yaw offset. In full wake situations, fore-after loads increase with yaw offsets on both sides with even larger fatigue in the positive direction. On the contrary, in partial wake conditions, the fore-after DEL decreases for both positive and negative yaw angles with the maximum value at non-yawed state. The commonality is that positive yaw offsets would lead to a greater load increase.

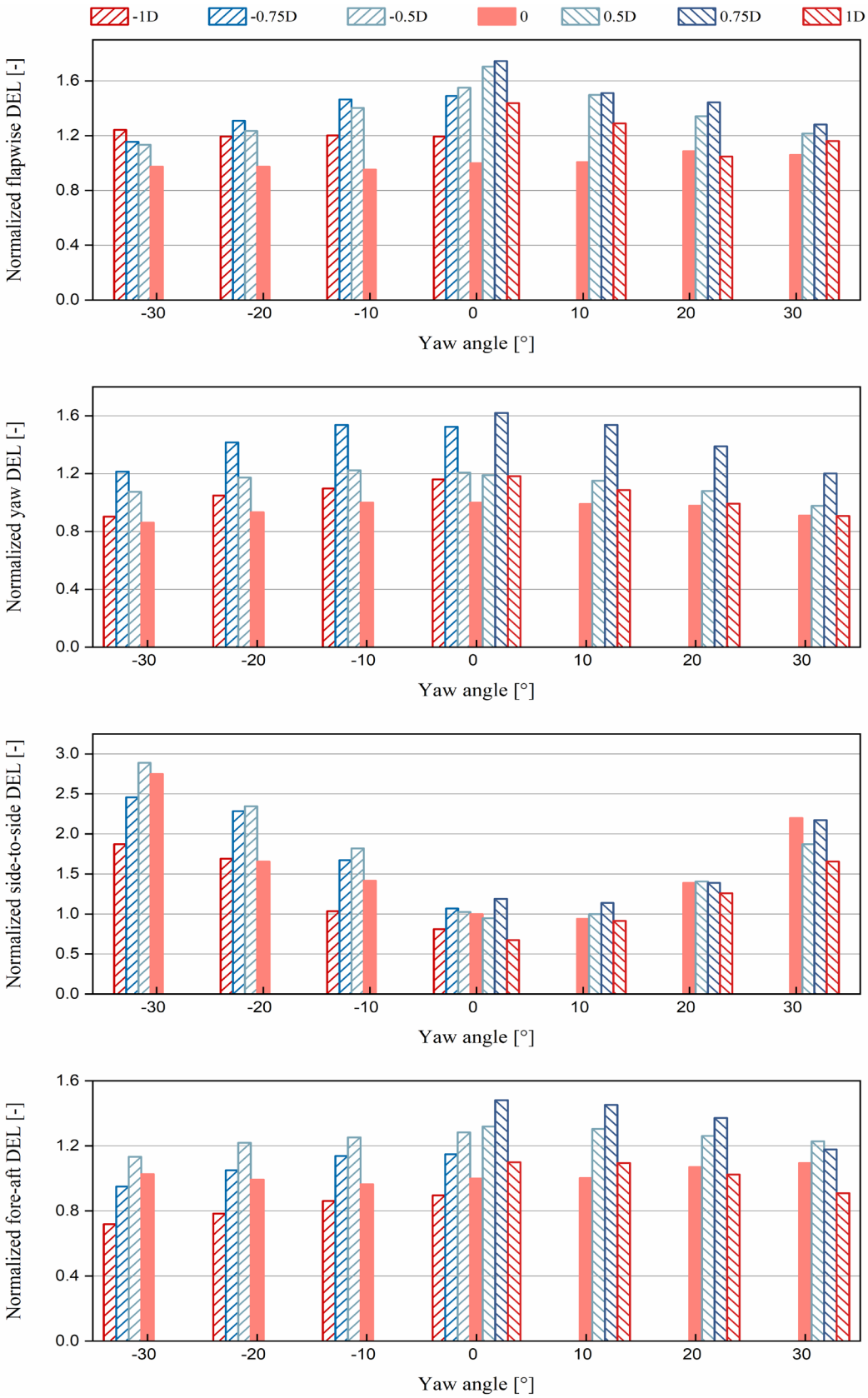

Fig.13 Fatigue loads variation as a function of yaw angle under partial wake effects.

5. The determination of optimal yaw angle

The trends of different fatigue loads and power yield are analyzed with respect to yaw offsets and different inflow conditions. It is found that although some fatigue loads may decrease with yaw offset, there is a penalty in power yield. Therefore, an efficient yaw control strategy considering both structural responses and power yields need to be further investigated.

In this study, a cost function is proposed to fully involve the fatigue loads of all critical turbine components from the blade root to yaw bearing, and tower base. It can be defined as the ratio of the averaged value of these equivalent fatigue loads to power yield both normalized by the values in their non-yawed cases. Moreover, since the maximal load at blade root does not necessarily appear at flapwise (0 degree) or edgewise (90 degrees) direction, the load rose algorithm [5] is employed in order to find the effective DEL at blade root DEL_{BR}. According to the IEC standard, 12 sectors are set with an interval of 15° and the load from the sector with largest contribution will be adopted. Similarly, the resultant bending moment at tower base DEL_{TB} can be obtained. Therefore, the cost function can be given as:

$$Cost\ Function(\gamma) = \frac{\left(\frac{DEL_{BR}(\gamma)}{DEL_{BR}(0°)} + \frac{DEL_{Yawing}(\gamma)}{DEL_{Yawing}(0°)} + \frac{DEL_{TB}(\gamma)}{DEL_{TB}(0°)} \right) \Big/ 3}{\frac{Power(\gamma)}{Power(0°)}} \tag{6}$$

where γ is the yaw angle.

The optimal yaw angle can be defined as:

$$\gamma_{opt} = \arg\min_{\gamma}(Cost\ Function(\gamma)) \tag{7}$$

To our best knowledge, it is the first cost function of yaw control that considers all critical turbine components and adopts resultant fatigue loads instead of just simple additions.

Fig. 14 displays the trend of cost function with respect to yaw offsets under different

wind speeds and a shear exponent of 0.18. The structural performance and power generation that do not appear in the fatigue analysis above are taken from the author's previous study [22]. It can be seen that yaw offsets in the positive direction usually have a lower "cost" than the negative counterpart. A cost value lower than one denotes an efficient yaw range that has considerable load reduction and little power loss. As shown in this figure and Table 4, the efficient yaw ranges all appear in the positive yaw direction and will be expanded as the speed increases. Considering the symmetrical distribution of power output as a function of yaw angle, positive yaw control is proved to be beneficial for structural performance in terms of the whole turbine. In addition to a larger efficient yaw range, greater wind speeds also result in a gentler slope of the cost function with respect to yaw offsets, which can be explained by relatively small power losses when yaw operates. On the contrary, large yaw offsets at lower speeds are considered detrimental to the turbine performance.

According to Eq. (7), the optimal yaw angle corresponds to where the cost function has the minimal value. As shown in Table 4, the optimal yaw angle of wind speeds under rated speed is 5° and increases to 10° as inflow speed greater than 11.4m/s. It should be noted that the specific value may vary depending on different inflow conditions including speed, shear exponent, and turbulent intensity, but qualitative law would remain as discussed above.

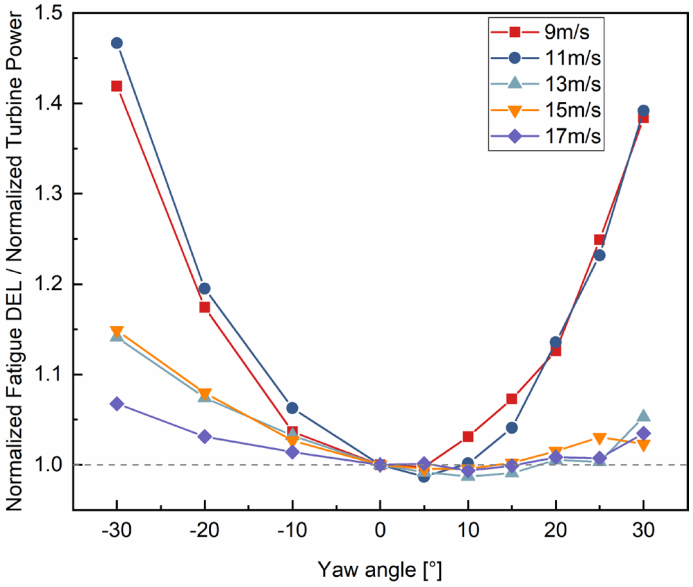

Fig.14 Normalized power yield with a cost of fatigue loads.

Table 4 Optimal yaw angles at different inflow speeds.

Inflow speed [m/s]	9	11	13	15	17
Efficient yaw range [°]	0~6	0~10	0~17	0~15	0~15
Optimal yaw angle [°]	5	5	10	10	10

6. Conclusion

This paper gives a comprehensive fatigue analysis of wind turbines under yaw control and the combined effect of yaw control and wake. Various inflow conditions, including both sheared inflows and wake flows, combined with practical yaw operations are employed to investigate the structural responses of critical turbine components. Afterwards, a cost function is proposed for the first time to determine the optimal yaw angle by fully considering the fatigue loads of the target WT. The main conclusions can be summarized as follows.

(1) Except for edgewise moment and power output, increasing turbulent levels can substantially increase the fatigue loads and the effects of yaw offsets on tower base loads, while decreasing the effects of yaw offsets on the loads at blade root and yaw bearing. Besides, strong shear inflows are found to have little effect on the mechanical loads at tower base and power yield but can significantly increase the loads related to blade and yaw bearing.

(2) The load magnitudes of yawed WTs under full wake are mostly larger than those under free stream except for the flapwise moment, which indicates that the increased turbulent intensity outweighs the decreased wind speed on fatigue loads. Moreover, the load trends are different from those under free flow. The flapwise and fore-aft DEL almost monotonically increase with yaw offsets and the yaw moment has the opposite load trend compared with the sheared flow counterpart. As for the side-to-side load

trend, larger loads at negative yaw offsets change the original nearly symmetrical distribution.

(3) Due to the different inflow characteristics, the fatigue loads caused by yaw under partial wake are different from that under full wake. The asymmetric inflow distribution in the partial wake is found to outweigh the reduced turbulence in blade fatigue. The most significant increase of yaw DEL appears at $\pm 0.75D$, where the rotor experiences approximately half wake and half sheared flow. All partial wake cases concerning side-to-side moment follow a similar load trend to the full wake cases while the fore-after load trend is changed with a remarkable load increase in positive yaw offsets.

(4) The efficient yaw control region all appears at positive yaw direction, which indicates that positive yaw offsets induce fewer fatigue loads than the negative counterparts. With the increase in inflow speeds, the efficient region is enlarged from 0°~6° at wind speed of 9m/s to about 0°~15° at above-rated wind speeds. Similarly, the optimal yaw angle at below-rated speeds is 5° and increases to 10° when the speeds are larger than the rated value.

The combined effects of wake and yaw control on wind turbine fatigue loads conducted in this paper and the proposed cost function are expected to make contributions to the active yaw control strategy in wind farms.

Declaration of Competing Interest

The authors declare that they have no known competing financial interests or personal relationships that could have appeared to influence the work reported in this paper.

Acknowledgment

The work described in this paper was supported by the Research Institute for Sustainable Urban Development (RISUD) with the account number of BBW8 and the FCE Dean Research project with the account number of ZVHL, The Hong Kong Polytechnic University.

References

[1] Lee J, Zhao F. GWEC Global Wind Report. Glob Wind Energy Counc 2022:75.

[2] He R, Yang H, Sun H, Gao X. A novel three-dimensional wake model based on anisotropic Gaussian distribution for wind turbine wakes. Appl Energy 2021;296:117059.

[3] He R, Sun H, Gao X, Yang H. Wind tunnel tests for wind turbines: A state-of-the-art review. Renew Sustain Energy Rev 2022;166:112675.

[4] Yang J, Fang L, Song D, Su M, Yang X, Huang L, et al. Review of Control Strategy of Large Horizontal-axis Wind Turbines Yaw System n.d.:1–33.

[5] Damiani R, Dana S, Annoni J, Fleming P, Roadman J, Van Dam J, et al. Assessment of wind turbine component loads under yaw-offset conditions. Wind Energy Sci 2018;3:173–89. https://doi.org/10.5194/wes-3-173-2018.

[6] Paul Fleming1, Pieter M.O. Gebraad2, Sang Lee1, Jan-Willem van Wingerden2, Kathryn Johnson1, Matt Churchfield1, John Michalakes1 PS and PM. Simulation comparison of wake mitigation control strategies for a two-turbine case. Wind Energy 2013:1–20. https://doi.org/10.1002/we.

[7] Akay B, Ragni D, Ferreira CS, Bussel GJW Van. Load alleviation of wind turbines by yaw misalignment. Wind Energy 2013:1–20. https://doi.org/10.1002/we.

[8] Fleming PA, Gebraad PMO, Lee S, van Wingerden JW, Johnson K, Churchfield M, et al. Evaluating techniques for redirecting turbine wakes using SOWFA. Renew Energy

2014;70:211–8. https://doi.org/10.1016/j.renene.2014.02.015.

[9] Shen X, Zhu X, Du Z. Wind turbine aerodynamics and loads control in wind shear flow. Energy 2011;36:1424–34. https://doi.org/10.1016/j.energy.2011.01.028.

[10] Jeong MS, Kim SW, Lee I, Yoo SJ, Park KC. The impact of yaw error on aeroelastic characteristics of a horizontal axis wind turbine blade. Renew Energy 2013;60:256–68. https://doi.org/10.1016/j.renene.2013.05.014.

[11] Ke S, Wang T, Ge Y, Wang H. Wind-induced fatigue of large HAWT coupled tower–blade structures considering aeroelastic and yaw effects. Struct Des Tall Spec Build 2018;27:1–14. https://doi.org/10.1002/tal.1467.

[12] Zong H, Porté-Agel F. A momentum-conserving wake superposition method for wind farm power prediction. J Fluid Mech 2020;889:1–15. https://doi.org/10.1017/jfm.2020.77.

[13] Chanprasert W, Sharma RN, Cater JE, Norris SE. Large Eddy Simulation of wind turbine fatigue loading and yaw dynamics induced by wake turbulence. Renew Energy 2022;190:208–22. https://doi.org/10.1016/j.renene.2022.03.097.

[14] Sun J, Chen Z, Yu H, Gao S, Wang B, Ying Y, et al. Quantitative evaluation of yaw-misalignment and aerodynamic wake induced fatigue loads of offshore Wind turbines. Renew Energy 2022;199:71–86. https://doi.org/10.1016/j.renene.2022.08.137.

[15] Urbán AM, Larsen TJ, Larsen GC, Held DP, Dellwik E, Verelst D. Optimal yaw strategy for optimized power and load in various wake situations. J Phys Conf Ser 2018;1102. https://doi.org/10.1088/1742-6596/1102/1/012019.

[16] Lin M, Porté-Agel F. Power Maximization and Fatigue-Load Mitigation in a Wind-turbine Array by Active Yaw Control: An les Study. J Phys Conf Ser 2020;1618. https://doi.org/10.1088/1742-6596/1618/4/042036.

[17] Campagnolo F, Petrović V, Bottasso CL, Croce A. Wind tunnel testing of wake control strategies. Proc Am Control Conf 2016;2016-July:513–8. https://doi.org/10.1109/ACC.2016.7524965.

[18] Bossanyi E. Combining induction control and wake steering for wind farm energy and fatigue loads optimisation 2018.

[19] van Dijk MT, van Wingerden JW, Ashuri T, Li Y. Wind farm multi-objective wake redirection for optimizing power production and loads. Energy 2017;121:561–9. https://doi.org/10.1016/j.energy.2017.01.051.

[20] Ennis BL, White JR, Paquette JA. Wind turbine blade load characterization under yaw offset at the SWiFT facility. J Phys Conf Ser 2018;1037. https://doi.org/10.1088/1742-6596/1037/5/052001.

[21] J. Jonkman, S. Butterfield, W. Musial and GS. Definition of a 5-MW Reference Wind Turbine for Offshore System Development. J Offshore Mech Arct Eng 2018;140. https://doi.org/10.1115/1.4038580.

[22] He R, Yang H, Sun S, Lu L, Sun H, Gao X. A machine learning-based fatigue loads and power prediction method for wind turbines under yaw control. Appl Energy 2022;326:120013.

[23] Kanev SK, Savenije FJ. Active Wake Control : loads trends. Tech Report, ECN-E--15-004 2015.

[24] Jonkman BJ, Kilcher L. TurbSim User's Guide. Natl Renew Energy Lab 2012:1–87.

[25] Infrastructure N, Centre SC, Infrastructure N, Reference D, Great Britain. Centre for the Protection of National Infrastructure, Murray-webster R, et al. IEC International Standard 61400-1 2005;2005:88.

[26] Conti D, Dimitrov N, Peña A, Herges T. Probabilistic estimation of the Dynamic Wake

Meandering model parameters using SpinnerLidar-derived wake characteristics. Wind Energy Sci 2021;6:1117–42.

[27] Jonkman J, Shaler K. FAST . Farm User ' s Guide and Theory Manual 2020.

[28] Reinwardt I, Gerke N, Dalhoff P, Steudel D, Moser W. Validation of wind turbine wake models with focus on the dynamic wake meandering model. J Phys Conf Ser 2018;1037. https://doi.org/10.1088/1742-6596/1037/7/072028.

[29] Jonkman J, Annoni J, Hayman G, Jonkman B, Purkayastha A. Development of FAST.Farm: A new multiphysics engineering tool for wind farm design and analysis. 35th Wind Energy Symp 2017 2017. https://doi.org/10.2514/6.2017-0454.

[30] Wingerden JW Van, Ruben SD, Marden JR, Pao LY. Wind plant power optimization through yaw control using a parametric model for wake effects—a CFD simulation study 2016:95–114. https://doi.org/10.1002/we.

[31] Mendez Reyes H, Kanev S, Doekemeijer B, van Wingerden J-W. Validation of a lookup-table approach to modeling turbine fatigue loads in wind farms under active wake control. Wind Energy Sci 2019;4:1–19. https://doi.org/10.5194/wes-2019-34.

[32] Larsen TJ, Larsen GC, Pedersen MM, Enevoldsen K, Madsen HA. Validation of the Dynamic Wake Meander model with focus on tower loads. J Phys Conf Ser 2017;854. https://doi.org/10.1088/1742-6596/854/1/012027.

[33] Yang Y, Bashir M, Wang J, Yu J, Li C. Performance evaluation of an integrated floating energy system based on coupled analysis. Energy Convers Manag 2020;223:113308. https://doi.org/10.1016/j.enconman.2020.113308.

[34] Clark CE, Barter G, Shaler K, DuPont B. Reliability-based layout optimization in offshore wind energy systems. Wind Energy 2021:1–24. https://doi.org/10.1002/we.2664.

[35] Luna J, Falkenberg O, Gros S, Schild A. Wind turbine fatigue reduction based on economic-tracking NMPC with direct ANN fatigue estimation. Renew Energy 2020;147:1632–41. https://doi.org/10.1016/j.renene.2019.09.092.

[36] Wu K, Zhou H, An S, Huang T. Optimal coordinate operation control for wind-photovoltaic-battery storage power-generation units. Energy Convers Manag 2015;90:466–75. https://doi.org/10.1016/j.enconman.2014.11.038.

[37] Miner MA. Cumulative damage in fatigue 1945.

[38] Hang Menga, 1, Xin Yua SC. Numerical investigations on fatigue loading of yaw-based control for large wind turbines in an offshore wind farm. Int J GREEN ENERGY 2019;173:794–801. https://doi.org/10.1016/j.oceaneng.2019.01.042.

[39] Boorsma K. Power and loads for wind turbines in yawed conditions. ECN 2012.